PCCP

Experimental and theoretical study of the F, Cl and Br reactions with formaldehyde and acetaldehyde

J. A. Beukes, B. D'Anna, V. Bakken and C. J. Nielsen*

Department of Chemistry, University of Oslo, P.O. Box 1033 Blindern, N-0315 Oslo, Norway. E-mail: claus.nielsen@kjemi.uio.no

Received 7th June 2000, Accepted 7th July 2000
Published on the Web 10th August 2000

The vapour phase reactions of formaldehyde, formaldehyde-d_2, ^{13}C-formaldehyde, acetaldehyde, acetaldehyde-1-d_1, acetaldehyde-2,2,2-d_3, and acetaldehyde-d_4 with Cl and Br atoms were studied at 298 ± 2 K and 1013 ± 10 hPa using long-path FTIR detection. For formaldehyde the only products observed were HCl, HBr and CO; for acetaldehyde the product distribution suggests one dominant channel: $CH_3CHO + X \rightarrow CH_3CO + HX$. The kinetic isotope effects at 298 K were determined by the relative rate method as: $k_{Cl+HCHO}/k_{Cl+DCDO} = 1.302 \pm 0.014$, $k_{Cl+H^{13}CHO}/k_{Cl+DCDO} = 1.217 \pm 0.025$, $k_{Br+HCHO}/k_{Br+DCDO} = 7.5 \pm 0.4$ and $k_{Br+H^{13}CHO}/k_{Br+DCDO} = 6.8 \pm 0.4$, $k_{Cl+CH_3CHO}/k_{Cl+CH_3CDO} = 1.343 \pm 0.023$, $k_{Cl+CH_3CHO}/k_{Cl+CD_3CDO} = 1.323 \pm 0.018$, $k_{Cl+CD_3CHO}/k_{Cl+CH_3CDO} = 1.345 \pm 0.015$, $k_{Cl+CD_3CHO}/k_{Cl+CD_3CDO} = 1.394 \pm 0.021$, $k_{Br+CH_3CHO}/k_{Br+CH_3CDO} = 3.98 \pm 0.26$, $k_{Br+CH_3CHO}/k_{Br+CD_3CDO} = 3.79 \pm 0.29$, $k_{Br+CD_3CHO}/k_{Br+CH_3CDO} = 4.02 \pm 0.10$ and $k_{Br+CD_3CHO}/k_{Br+CD_3CDO} = 3.96 \pm 0.20$. Quoted errors represent 3σ from the statistical analyses and do not include possible systematic errors. The reactions of F, Cl and Br atoms with formaldehyde and acetaldehyde were studied by quantum chemical methods on the MP2 level of theory using the cc-pVDZ basis sets. The calculations indicate the existence of a weak adduct in which the halogen atoms are bonded to the aldehydic oxygen. Transition states of the reactions $X + HCHO \rightarrow HX + CHO$ and $X + CH_3CHO \rightarrow HX + CH_3CO$ (X = F, Cl, Br) were located. Reaction rate coefficients and kinetic isotope effects, calculated from conventional transition state theory are compared to experimental data and the deviations are tentatively attributed to adduct formation.

Introduction

Formaldehyde and acetaldehyde are key components in the chemistry of the atmosphere. Both have natural sources (vegetation, forest fires and microbiological processes);[1] they are also primary pollutants, produced by partial oxidation of hydrocarbon fuels, and secondary pollutants, produced by oxidation of volatile organic compounds in the troposphere. Their concentration outside urban areas can be quite high, ranging from 1–25 μg m^{-3} (1–20 ppb HCHO).[1] The tropospheric loss processes include photolysis from solar irradiation, reaction with OH radicals, Cl and Br atoms during the daytime, or reaction with NO_3 radicals during the night-time. Reactions with Cl and Br atoms are important in the marine boundary layer and sometimes the Br reaction constitutes the major formaldehyde loss process.[2] Formaldehyde is also an important species in the stratosphere where it, as in the Arctic troposphere, reduces the chain length of the Br catalytic ozone destruction cycle.[3,4] The reaction of fluorine atoms with formaldehyde is only of minor importance in the stratosphere where methane constitutes the major fluorine sink.

The present study was initially undertaken because the gas-phase reactivity of aldehydes towards OH and NO_3 radicals apparently deviated from the expected linear free energy relationship typical of abstraction reactions.[5] Preliminary studies of the kinetic isotope effects in the reactions of Cl and OH with formaldehyde also indicated similarities in their reaction mechanisms.[6]

Kinetic data for the reactions $X + HCHO \rightarrow$ "products" have previously been obtained by several methods: X = F,[7] Cl[8–14] and Br.[7,10,15] The kinetic isotope effect in the Cl reaction with HCHO/DCDO, $k_{Cl+HCHO}/k_{Cl+DCDO}$, was reported as 1.3.[8] We have recently reported an unusually large kinetic isotope effect in the bromine–formaldehyde reaction, with a ratio of $k_{Br+HCHO}/k_{Br+DCDO}$ around 7.[16] There are also several reports on the kinetics of the reactions $X + CH_3CHO \rightarrow$ "products": X = F,[17–19] Cl,[12,20–24] and Br.[25–31]

Experimental

Instrumentation

The experiments were performed in synthetic air (AGA plus; CO, $NO_x < 100$ ppb, C_nH_m, <1 ppm) at 298 ± 2 K and 1013 ± 10 hPa in a 250 L electropolished stainless-steel reactor equipped with a White-type multiple reflection mirror system of 120 m optical path-length for on-line FTIR detection. Infrared spectra were recorded with a Bruker IFS 88 employing a nominal resolution of 0.5 cm^{-1}, Happ–Genzel apodization, and adding 100 scans; the recording time of the spectrum was *ca.* 75 s. Chlorine and bromine atoms were produced by photolysis of molecular chlorine or bromine employing Philips TLD-08 fluorescence lamps ($\lambda_{max} \sim 370$ nm) mounted in a quartz tube and inserted into the reaction chamber; the lamps were turned off during registration of the spectra. Typical reactant volume fractions were: formaldehyde, 0.5 ppm; acetaldehyde, 2 ppm; Cl_2 and Br_2, 2–10 ppm.

The chemical and photolytical stability of the aldehydes in the reaction chamber was investigated separately; the compounds showed lifetimes of the order of days in the reaction chamber. The deuterated acetaldehydes showed a strong tendency to form trimers in the liquid phase (acid catalysed). The trimer–monomer equilibrium is strongly shifted towards the

monomeric form in the vapour phase, but it took hours for a complete conversion from trimer to monomer to take place. Before each series of relative rate experiments a blind test with only the oxidant precursor was carried out to ensure that formaldehyde or acetaldehyde were not produced by oxidation of impurities either present in the synthetic air or adsorbed on the cell walls.

Chemicals

Cl_2 and Br_2 were standard laboratory-grade chemicals. Formaldehyde (paraformaldehyde) and acetaldehyde were standard commercial samples with purity better than 98%. Paraformaldehyde-d_2 (99.8 atom% D), acetaldehyde-1-d_1 (98 atom% D), -2,2,2-d_3 (98.8 atom% D) and -d_4 (99.6 atom% D) were obtained from CDN Isotopes. ^{13}C formaldehyde (99 atom% ^{13}C) was from ISOTEC Inc.

Quantum chemical computations

All computations were carried out using GAUSSIAN 98.[32] The standard method consisted of a Hartree–Fock calculation followed by a second-order Møller–Plesset correlation energy correction,[33–39] excluding inner-shells (frozen core). Dunning's medium-sized correlation consistent basis sets, cc-pVDZ,[40–44] which include polarisation functions, were chosen to obtain reasonably accurate geometries and relative energies. Additional calculations were carried out including the inner-shells in the correlation calculation and with diffuse functions added through the use of the aug-cc-pVDZ basis sets.[40,41]

Results and discussion

Product study

Three channels may be envisaged for the F, Cl and Br reactions with formaldehyde:

$$X + HCHO \rightarrow H + XCHO \quad (Ia)$$

$$\rightarrow HX + CHO \quad (Ib)$$

$$\rightarrow HX + H + CO \quad (Ic)$$

Under atmospheric conditions reactions (Ib) and (Ic) will immediately be followed by reaction of H or HCO with O_2 leading to CO and HO_2, and both channels therefore result in the same final products. The available experimental reaction enthalpies are compared to the results from quantum chemistry (see later) in Table 1. As can be seen, fluorine may open all three channels, chlorine channels (Ib) and (Ic), while bromine only will react through channel (Ib) under atmospheric conditions.

As mentioned above the initial step in the oxidation of formaldehyde eventually leads to formation of HO_2 radicals:

$$HCO + O_2 \rightarrow C + HO_2 \quad (IIa)$$

$$H + O_2 \xrightarrow{M} HO_2 \quad (IIb)$$

The HO_2 radicals produced in reaction (II) enter a reversible equilibrium (III) to form a formaldehyde adduct.[46–52] This adduct can react irreversibly in several ways, of which the more important under the conditions in our reactor are given below, and thereby introduce a significant additional loss channel for formaldehyde:[46,47]

$$HCHO + HO_2 \rightleftharpoons HOO\text{–}C_2\text{–}O \rightarrow HO\text{–}CH_2\text{–}OO \quad (III)$$

$$HO\text{–}CH_2\text{–}OO + HO_2 \rightarrow HO\text{–}CH_2\text{–}OOH + O_2 \quad (IVa)$$

$$\rightarrow HCOOH + H_2O + O_2 \quad (IVb)$$

$$2HO\text{–}CH_2\text{–}OO \rightarrow HO\text{–}CH_2OH + HCOOH + O_2 \quad (Va)$$

$$\rightarrow 2HO\text{–}CH_2\text{–}O + O_2 \quad (Vb)$$

$$HO\text{–}CH_2\text{–}O + O_2 \rightarrow HCOOH + HO_2 \quad (VI)$$

In addition, there is always NO_x present in the synthetic air used (<100 ppb). O_3 and OH radicals will therefore also be generated during the photochemical reactions; the O_3 reaction with formaldehyde is far too slow to be of importance in the reactor, but OH might contribute to the degradation. The photodecomposition of O_3 at 370 nm is sufficiently slow compared to the timescale of the experiment that its strong IR band around 1050 cm^{-1} should be clearly detectable if more than 50 ppb was formed. This band was never observed, nor did we see the NO band around 1875 cm^{-1} and only traces of NO_2 were seen around 1620 cm^{-1}. Of the oxidation products formed in reactions (IV) to (VI) only formic acid is thermally stable and it can thus be used as an indicator of the additional formaldehyde loss through HO_2. When using volume fractions of formaldehyde below 1 ppm and halogen volume fractions below 5 ppm the amount of formic acid formed was below our detection limit (~10 ppb). Examples of the obtained spectra are given in Fig. 1 and 2 showing the C–H and C–D stretching regions, respectively, from an experiment with 0.6 ppm H ^{13}CHO, 0.4 ppm DCDO and 3.0 ppm Cl_2 in purified air. Although there are no traces in the spectra of formylchloride, with its characteristic and very strong ν_{CO} and ν_{CCl} bands around 1784 and 739 cm^{-1}, respectively, we cannot

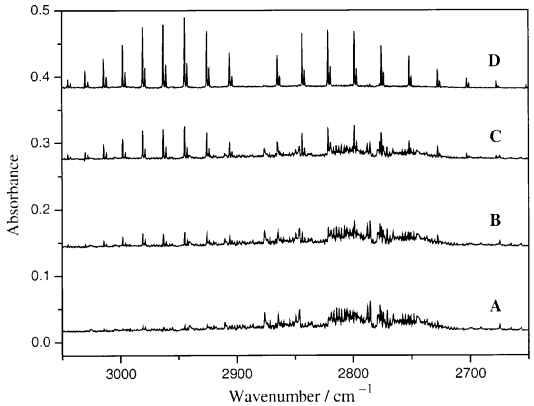

Fig. 1 IR spectra of the C–H stretching region of a 0.6 ppm H ^{13}CHO, 0.4 ppm DCDO and 3.0 ppm Cl_2 mixture obtained at different photolysis times. The bands are mainly due to H ^{13}CHO and HCl. (A) Before photolysis; (B) after 120 s photolysis; (C) after 360 s photolysis; (D) after 870 s photolysis.

Table 1 Enthalpies of reaction at 298 K (in kJ mol^{-1}) for the reactions of halogen atoms with formaldehyde[a]

	F		Cl		Br	
X + XCHO →	Obs.	Calc.[c]	Obs.	Calc.	Obs.	Calc.
H + XCHO	−145.3[b]	−148.1		8.5		57.2
HX + CHO	−202.3	−183.0	−63.2	−57.4	2.2	−10.3
HX + H + CO	−136.6	−151.8	2.5	−26.3	67.9	20.9

[a] Based on available experimental data in ref. 45 (and references therein). [b] Calculated from $\Delta_r H°$ (0 K). [c] Results from MP2/cc-pVDZ calculations, see text.

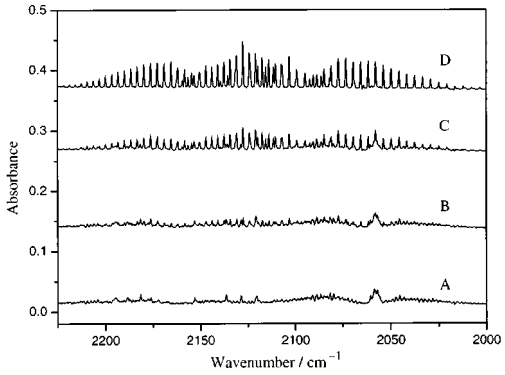

Fig. 2 IR spectra of the C–D stretching region of a 0.6 ppm H ^{13}CHO, 0.4 ppm DCDO and 3.0 ppm Cl_2 mixture obtained at different photolysis times. The bands are mainly due to DCDO, CO and ^{13}CO. (A) Before photolysis; (B) after 120 s photolysis; (C) after 360 s photolysis; (D) after 870 s photolysis.

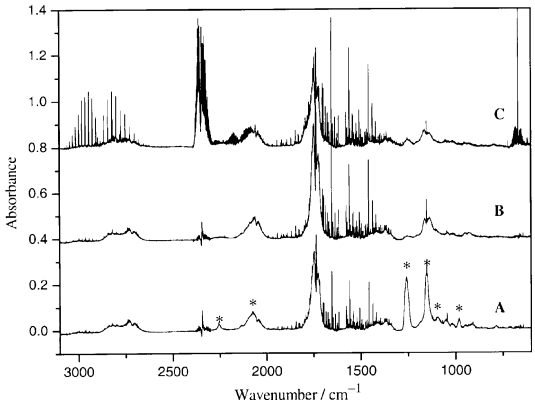

Fig. 3 IR survey spectra of a 2.2 ppm CH_3CHO, 2.2 ppm CD_3CDO and 7.0 ppm Cl_2 mixture obtained at different times in the reactor. (A) Immediately after mixing, bands marked with asterisks are due to $(CD_3CDO)_3$; (B) after 2 h in the cell; (C) after 1300 s photolysis.

state from the spectroscopic evidence alone that chlorine reacts exclusively through channel (Ib). To be discussed later, the theoretical calculations seem to rule out the other path.

In principle, the halogen atoms may react in similar ways with acetaldehyde as with formaldehyde, and in addition also by hydrogen abstraction from the methyl group:

$$X + CH_3CHO \rightarrow CH_3CXO + H \quad \text{(VIIa)}$$

$$\rightarrow CH_3 + XCHO \quad \text{(VIIa′)}$$

$$\rightarrow CH_3CO + HX \quad \text{(VIIb)}$$

$$\rightarrow CH_3 + HX + CO \quad \text{(VIIc)}$$

$$\rightarrow C_2CHO + HX \quad \text{(VIId)}$$

The available experimental reaction enthalpies are compared to the results from quantum chemistry (see later) in Table 2. As seen, fluorine may open all five channels, while bromine will react only through channel (VIIb) under atmospheric conditions. The latter is confirmed by this work and by previous experimental results.[27–29,31] For the fluorine reaction, only channels (VIIb), 65%, and (VIId), 35%, have so far been verified.[17] The thermodynamic data, Table 2, indicate that channels (VIIb–d) should be open to the chlorine reaction; the theoretical calculations suggest (VIId) to be endothermic, and previous studies also suggest that less than 5% of the Cl reaction proceeds this way at room temperature.[22,24]

IR survey spectra from the reaction of Cl atoms with a CH_3CHO and CD_3CDO mixture in purified air are given in Fig. 3, while Fig. 4 shows details of the C–H and C–D stretching regions. As just mentioned, previous studies conclude that channel (VIId), constitutes less than 5% of the total reaction.[22,24] The present spectra show that the only compounds formed in any substantial amount in the Cl reactions are HCHO, DCDO, HCl, DCl, CO_2 and CO. The spectra show no indications of the characteristic bands around 2835 and 1732 cm^{-1} from glyoxal (CHO–CHO), which is an expected oxidation product eventually resulting from path (VIId). This is a weighty argument on its own, as glyoxal is likely to react very fast with Cl atoms. In addition, glyoxal is not the only product formed following (VIId) formaldehyde and formyl radicals can also result. However, the product formation profiles, Fig. 5, observed in an experiment similar to the one mentioned above, but with a CH_3CHO–CH_3CDO mixture and Cl, show an excellent anti-correlation between the reacted acetaldehyde and the products formaldehyde and CO_2, while CO clearly is a secondary oxidation product (note that CO_2 is present from the start of the reaction). This product–time profile is only consistent with channel (VIIb) being the dominant pathway for the chlorine reaction with acetaldehyde at room temperature (the acetyl radical reacts quickly to generate HCHO and CO_2).

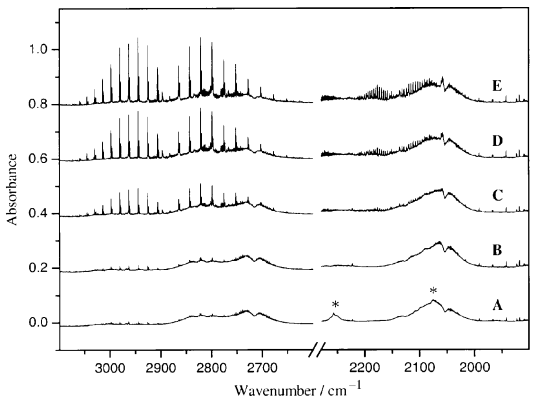

Fig. 4 IR spectra of a 2.2 ppm CH_3CHO, 2.2 ppm CD_3CDO and 7.0 ppm Cl_2 mixture obtained at photolysis different times. (A) Immediately after mixing, bands marked with asterisks are due to $(CD_3CDO)_3$; (B) after 2 h in the cell; (C) after 400 s photolysis; (D) after 850 s photolysis; (E) after 1300 s photolysis.

Table 2 Enthalpies of reaction at 298 K (in kJ mol^{-1}) for the reactions of halogen atoms with acetaldehyde[a]

	F		Cl		Br	
$X + CH_3CHO \rightarrow$	Obs.	Calc.[c]	Obs.	Calc.	Obs.	Calc.
$CH_3CXO + H$		−147.5		5.4		51.3
$CH_3 + XCHO$	−160.1[b]	−139.3		17.2		65.9
$CH_3CO + HX$	−211.2	−173.2	−72.1	−47.7	−6.7	−0.5
$CH_3 + HX + CO$	−151.4	−143.1	−12.3	−17.5	53.1	29.6
$CH_2CHO + HX$	−174.3	−108.9	−35.2	16.6	20.2	63.8

[a] Based on available experimental data in ref. 45 (and references therein). [b] Calculated from $\Delta_r H°$ (0 K). [c] Results from MP2/cc-pVDZ calculations, see text.

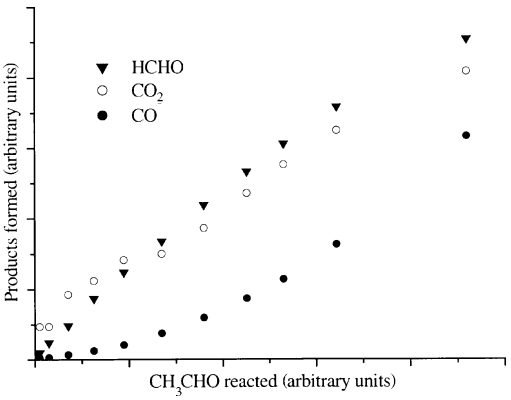

Fig. 5 Formation of oxidation products in the reaction of Cl atoms with CH_3CHO and CH_3CDO *vs.* amount of CH_3CHO reacted.

Kinetic study

The kinetic studies were carried out by the relative rate method, that is by considering two simultaneous bimolecular reactions with rate coefficients k_A and k_B:

$$\text{A} + \text{Radical} \xrightarrow{k_A} \text{Products}$$

$$\text{B} + \text{Radical} \xrightarrow{k_B} \text{Products}$$

Assuming that there are no other loss processes than the two above bimolecular reactions, then the following relation is valid:

$$\ln\left\{\frac{[A]_0}{[A]_t}\right\} = \frac{k_A}{k_B} \ln\left\{\frac{[B]_0}{[B]_t}\right\} \quad (1)$$

where $[A]_0$, $[A]_t$, $[B]_0$ and $[B]_t$ denote the concentrations of the compounds A and B at times zero and t, respectively. A plot of $\ln\{[A]_0/[A]_t\}$ *vs.* $\ln\{[B]_0/[B]_t\}$ will give the relative reaction rate coefficient $k_{rel} = k_A/k_B$ as the slope. The ratio between the concentrations of the compounds was found by spectral subtraction using spectra of the pure starting compounds, spectra of other compounds identified in the reaction mixture and a sloping background. Data from independent experiments were analysed jointly according to eqn. (1) using a weighted least-squares procedure including uncertainties in both reactant concentrations and allowing a zero-point offset.[53] The analyses are shown in Fig. 6 and 7 for the formaldehyde and acetaldehyde studies, respectively. The spectral ranges and the compounds included in the subtraction procedures are listed in Table 3, and the derived relative rates, with 3σ statistical errors, are given in Table 4. There is only one prior study of the kinetic isotope effect in this class of reactions, and the reported value for $k_{Cl+HCHO}/k_{Cl+DCDO} = 1.3 \pm 0.2$[8] is in excellent agreement with the present results.

The relative rate coefficients for the chlorine reactions are well determined, whereas the bromine reactions show larger uncertainties with 3σ errors of up to 8%. To be discussed below, there are additional errors inherent to the production of atoms and radicals in the system.

The program package FACSIMILE[54] was employed to simulate the complex set of reactions and the kinetics of the reactor system. In total, 102 thermal and 21 photolytic reactions were considered. The relevant thermal reactions and their rate coefficients were obtained from the NIST databases[55] and from a recent review of kinetic data for atmospheric modelling.[45] The rates of photolysis for Cl_2 and Br_2 in the cell were obtained in separate experiments. The photolysis rates of all other photolabile species were then obtained from the spectral characteristics of the irradiation lamps, data for quantum yields and absorption coefficients given by DeMore *et al.*,[56] and subsequent scaling according to the experimental photolysis rates for Cl_2 and Br_2.

The model calculations show that the amount of formaldehyde reacting *via* equilibrium (III) strongly depends upon the

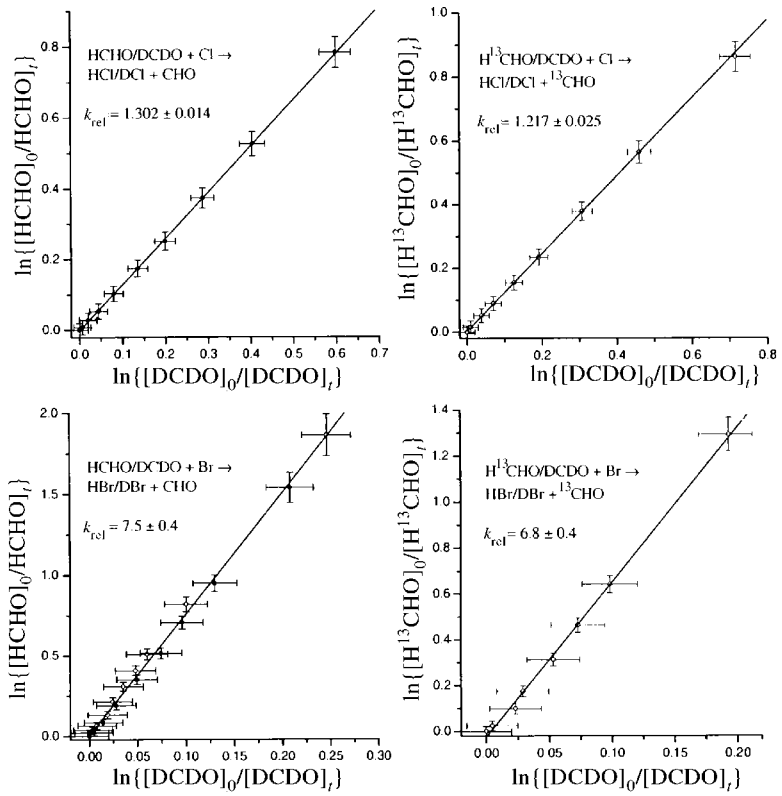

Fig. 6 Plots of $\ln\{[HCHO]_0/[HCHO]_t\}$ and $\ln\{[H\,^{13}CHO]_0/[H\,^{13}CHO]_t\}$ *vs.* $\ln\{[DCDO]_0/[DCDO]_t\}$ for the decays during reactions with Cl or Br atoms. The uncertainties ascribed to each data point are based on an estimated uncertainty in the subtraction procedure amounting to 2% of the initial concentration. The results are summarised in Table 4.

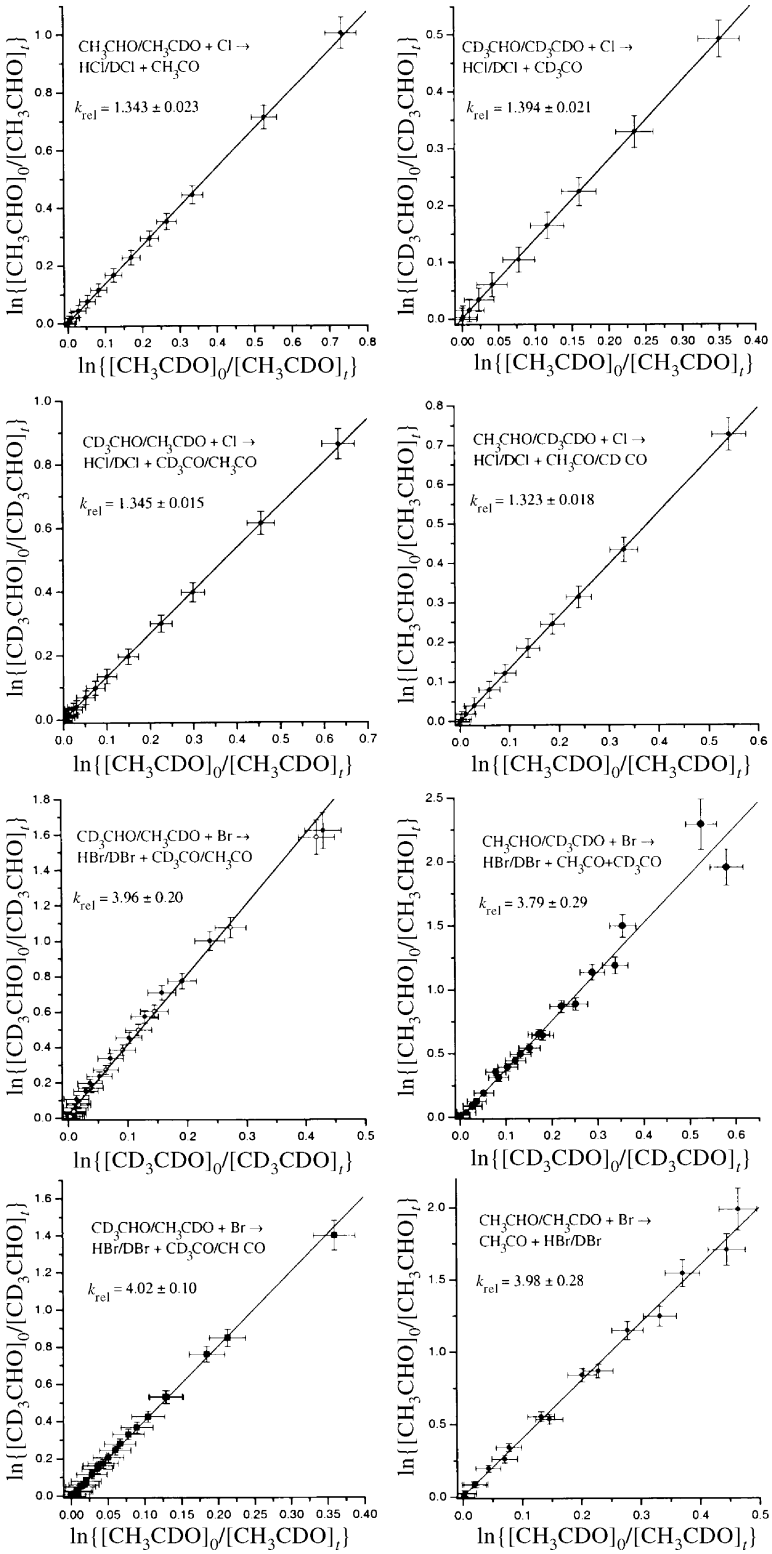

Fig. 7 Plots of $\ln\{[CH_3CHO]_0/[CH_3CHO]_t\}$ *vs.* $\ln\{[CH_3CDO]_0/[CH_3CDO]_t\}$, $\ln\{[CD_3CHO]_0/[CD_3CHO]_t\}$ *vs.* $\ln\{[CH_3CDO]_0/[CH_3CDO]_t\}$, $\ln\{[CD_3CHO]_0/[CD_3CHO]_t\}$ *vs.* $\ln\{[CD_3CDO]_0/[CD_3CDO]_t\}$, and $\ln\{[CH_3CHO]_0/[CH_3CHO]_t\}$ *vs.* $\ln\{[CD_3CDO]_0/[CD_3CDO]_t\}$, for the decays during reactions with Cl or Br atoms. The uncertainties ascribed to each data point are based on an estimated uncertainty in the subtraction procedure amounting to 2% of the initial concentration. The results are summarised in Table 4.

initial reactant concentrations. We have previously reported results from model calculations of the HCHO + Br reaction system and shown that the concentrations of the reactants should be in the sub-ppm range to minimise the HO_2 reactions.[16] Fig. 8 shows the results for a "worst case" scenario where 100 ppb NO_x in the bath gas is initially present as 99 ppb NO and 1 ppb NO_2 in a reaction mixture otherwise consisting of 0.5 ppm HCHO, 0.5 ppm DCDO and 2 ppm Cl_2. As can be seen, OH dominates the first minute of the reaction, but from then on the chlorine atom reaction completely dominates. In similar scenarios, but with less initial NO in the bath gas, the loss through HO_x is smaller.

We have used the simulation to estimate the propagation of error in the data analysis by ignoring the possible OH and HO_2 reactions with formaldehyde under similar conditions. For the HO_2 reaction with HCHO/DCDO (addition reaction)

Table 3 Wavenumber regions and additional reference compounds included in the spectral subtraction procedures

Compound	Wavenumber region used/cm^{-1}	Additional compounds used in spectral subtraction
HCHO	2850–2720	H_2O, D_2O HDO, HCl, HBr
$H^{13}CHO$	2850–2720	H_2O D_2O, HDO, HCl, HBr
DCDO	2100–2000	H_2O, CO, ^{13}CO
CH_3CHO	2850–2650	H_2O, D_2O HDO, HBr, HCHO, HCl
CH_3CDO	2100–2000	H_2O, D_2O, HDO, $(CH_3CDO)_3$, DCDO, CO, DBr, DCl
CD_3CHO	2850–2650	H_2O D_2O, HDO, HBr, HCl HCHO
CD_3CDO	2055–2000	H_2O, D_2O, HDO, DCDO, $(CD_3CDO)_3$, CO, DBr, DCl

the kinetic isotope effect is expected to be unity. For the OH reaction with HCHO/DCDO the kinetic isotope effect is somewhat larger than for Cl, but smaller than for Br.[57] The results show that the derived relative rates for the Cl and Br reactions with HCHO/DCDO are affected by less than 3% in the worst case scenario for low reactant concentrations. In the acetaldehyde experiments, the calculations show that the contribution from OH is smaller and can safely be ignored. In summary, the relative rates, which are reported in Table 4, are believed to be accurate within 10%.

Quantum chemical study: Electronic structure calculations

The most relevant minima and saddle points of the different room-temperature reactions were investigated at the MP2/cc-pVDZ and MP2/aug-cc-pVDZ levels of theory. Both frozen-core and full MP2 calculations were performed and fully optimised structures obtained without applying symmetry constraints.

Calculations were also done at the B3LYP/cc-pVDZ level for the Cl reactions. The DFT calculations with the B3LYP functional gave no barrier to the reaction Cl + HCHO → HCl + CHO. Comparing with both experimental and MP2 results, this is clearly not a correct description of the chemical reactions. B3LYP was therefore abandoned in favour of the MP2 calculations.

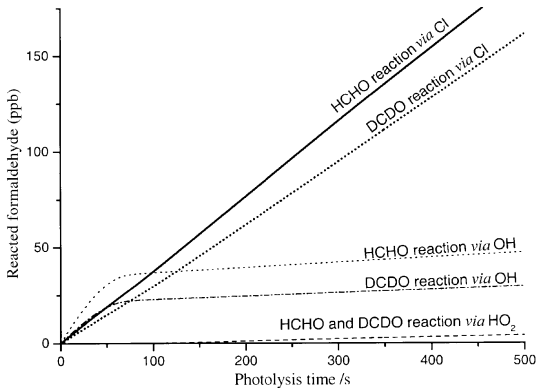

Fig. 8 "Worst case scenario" illustrating the contributions from different oxidants in the degradation of formaldehyde in the reactor. Results from modelling the reactions taking place in a mixture initially consisting of 0.5 ppm HCHO, 0.5 ppm DCDO, 2 ppm Cl_2, 99 ppb NO and 1 ppb NO_2, see text.

Effort was concentrated on the reaction pathway X + HCHO → HX + HCO, and the energies and structures of the relevant stationary points and transition states at the MP2/cc-pVDZ level are given in Fig. 9. For the sake of brevity, the more trivial molecular structures, radicals and atoms are not included. With the exception of the F···HCHO transition state, for which the calculations show a small barrier of *ca.* 0.9 kJ mol^{-1} to planarity, the other relevant structures are planar. The calculated electronic energies for separated reactants, adducts, transition states, minima and separated products for all three systems are given in Table 5. Energies are given in kJ mol^{-1} relative to the completely separated reactants (X + HCHO). A more exhaustive study of the potential energy surfaces will be undertaken at a later stage, and is likely to yield a number of stationary points with higher energy.

Structures calculated at the different levels of theory were practically identical, but as can be seen from Table 5, there were slight changes in the relative energies of the stationary points. Most notably the barriers to F and Cl reactions were lowered as the basis set was expanded and the level of correlation increased, giving results in better agreement with experiment, see below. It is likely that the outcome of similar calculations for the analogue reactions with acetaldehyde would be lower barriers to reactions here as well. Resources did not permit investigation of this or of the performance of even larger basis sets to check for convergence.

In addition to geometry optimisations of minima and saddle points, the potential energy surfaces were investigated further by performing relaxed potential energy scans from these stationary points. This was done for the fluorine and chlorine reactions to validate that the determined transition states connected the correct reactant and product configurations, as well as yielding reaction profiles for the different reactions. The reaction co-ordinate in the hydrogen abstraction X + HCHO → HX + HCO can described mainly by the X···HCHO distance "on the way in" and by the XH···CHO distance "on the way out" although other structural changes are also taking place. In the vicinity of the transition state the reaction co-ordinate is essentially just the hydrogen moving between two anchor points. The reaction profiles are shown in Fig. 10, and as seen, the potentials are

Table 4 Kinetic isotope effects in the reactions of halogen atoms with formaldehyde and acetaldehyde at 298 K

k_A/k_B	HCHO/DCDO	$H^{13}CHO$/DCDO	CH_3CHO/CH_3CDO	CH_3CHO/CD_3CDO	CD_3CHO/CH_3CDO	CD_3CHO/CD_3CDO
F	(2.864)[a]	(2.874)	(2.431)	(2.499)	(2.341)	(2.407)
Cl	1.302 ± 0.014	1.217 ± 0.025	1.343 ± 0.023	1.323 ± 0.018	1.345 ± 0.015	1.394 ± 0.021
	1.3 ± 0.2[8]	(2.545)	(1.639)	(1.593)	(1.665)	(1.618)
	(2.500)					
Br	7.5 ± 0.4	6.8 ± 0.4	3.98 ± 0.26	3.79 ± 0.29	4.02 ± 0.10	3.96 ± 0.20
	(5.698)	(5.929)	(2.190)	(2.149)	(2.231)	(2.190)

[a] Values in parentheses are calculated from conventional transition state theory using results from MP2/cc-pVDZ calculations, see text.

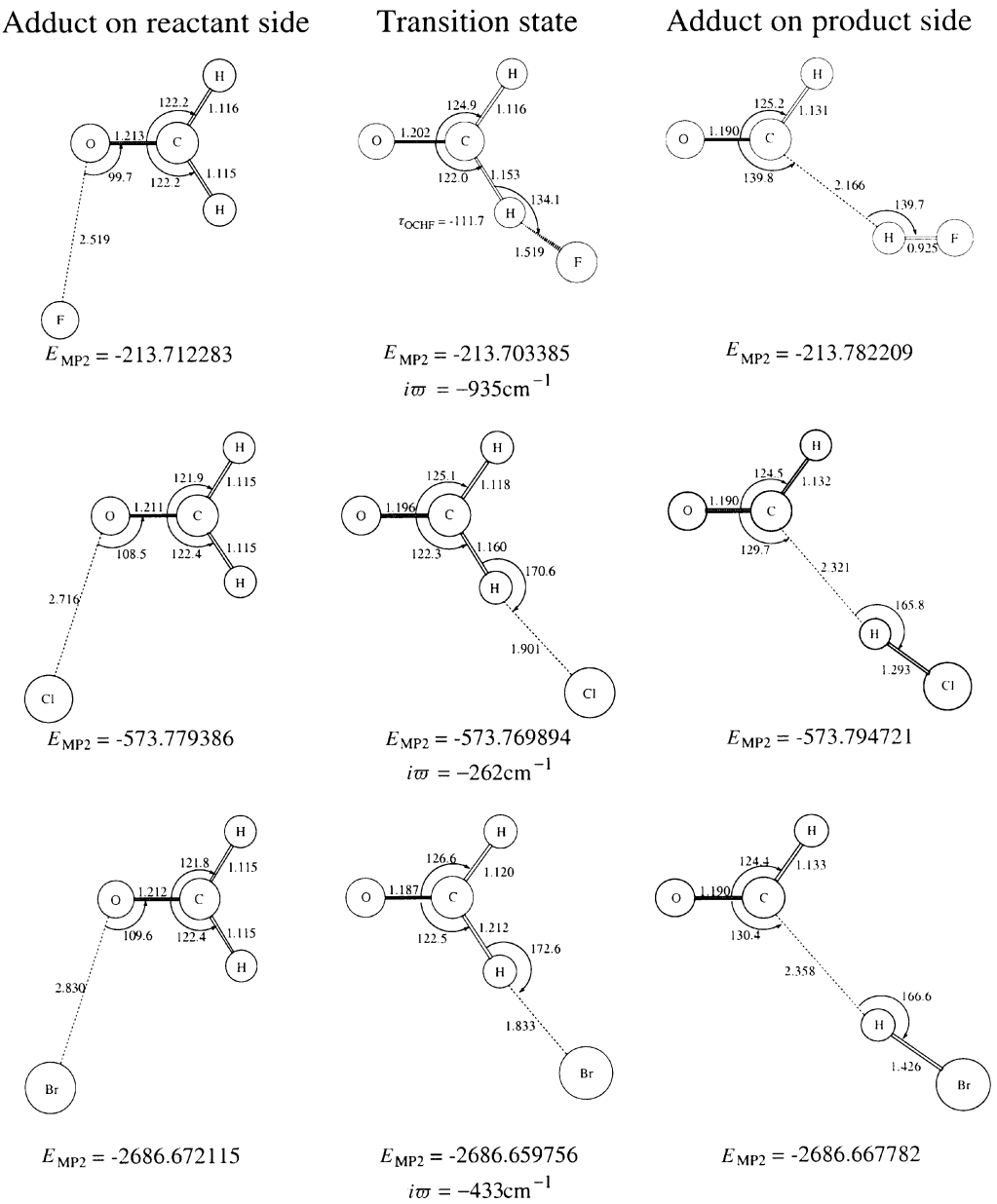

Fig. 9 Structures and electronic energies (in E_h) of adducts and transition states in the reactions; X + HCHO → CHO + HX; X = F, Cl, Br. With the exception of the F···HCHO transition state, all other structures are planar.

very shallow towards the product side. Back reaction should therefore be insignificant.

From the enthalpies of reaction, Table 1, it is clear that the X + HCHO → HX + HCO channel is open to all three systems. However, for fluorine the second reaction pathway (Ia) could be important, and for chlorine it is possible; this pathway, X + HCHO → H + XHCO, was therefore also investigated for fluorine and chlorine. It turned out that this

Table 5 Electronic energies of the reactions: X + HCHO → HX + CHO, X + HCHO → H + HX + CO and X + HCHO → H + XCHO (X = F, Cl, Br)

X	Level of computation	E_{X+HCHO} /E_h	ΔE_{Adduct} [a] /kJ mol^{-1}	ΔE_{TS} [a] /kJ mol^{-1}	ΔE_{min} [a] /kJ mol^{-1}	ΔE_{HX+HCO} /kJ mol^{-1}	$\Delta E_{H+HX+CO}$ /kJ mol^{-1}	
F	MP2(FC)/cc-pVDZ[b]	−213.703 384	−8.4	14.9	−192.0	−174.4	−126.2	−133.2
	MP2/cc-pVDZ	−213.715 561	−8.5	14.8	−191.9	−174.1	−125.4	−133.7
	MP2(FC)/aug-cc-pVDZ	−213.754 576	−7.5	9.0	−221.1	−205.5	−145.8	−142.8
	MP2/aug-cc-pVDZ	−213.761 863	−7.7	8.5	−221.3	−205.3	−145.0	−144.1
Cl	MP2(FC)/cc-pVDZ	−573.774 177	−13.7	11.2	−53.9	−42.2	5.9	27.6
	MP2/cc-pVDZ	−573.784 415	−14.0	10.7	−54.9	−43.0	5.7	26.7
	MP2(FC)/aug-cc-pVDZ	−573.811 027	−14.4	6.2	−59.1	−46.9	12.9	25.4
	MP2/aug-cc-pVDZ	−573.822 759	−15.5	4.4	−61.2	−48.0	12.2	23.5
Br	MP2(FC)/cc-pVDZ	−2686.666 312	−15.2	17.2	−3.9	6.8	55.0	77.6
	MP2/cc-pVDZ	−2686.678 309	—	—	—	6.1	54.8	—
	MP2(FC)/aug-cc-pVDZ	−2686.703 198	—	—	—	3.9	63.6	—
	MP2/aug-cc-pVDZ	−2686.717 744	—	—	—	2.4	62.6	—

[a] See Fig. 9. [b] FC, Frozen Core. For definition of basis sets, see ref. 40–44.

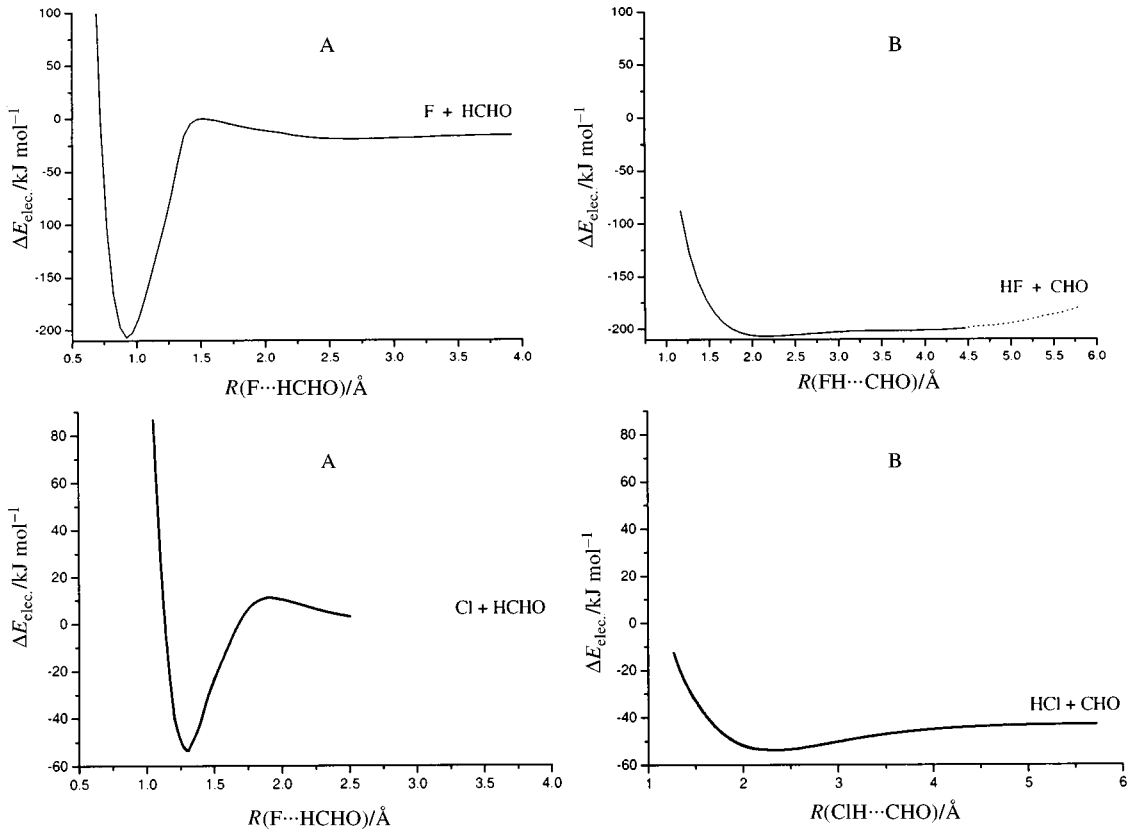

Fig. 10 Minimum potential energy curves for the reactions X + HCHO → CHO + HX; X = F, Cl. (A) Minimum potential energy as X approaches the aldehydic hydrogen; (B) minimum potential energy as HX leaves the formyl radical.

reaction path proceeds through two transition states, one between the reactants and a local, near tetrahedral CH_2XO minimum, and one between this minimum and the products, see Fig. 11. It was, unfortunately, not possible to locate the transition state between the reactants and the CH_2FO minima accurately. As the C–F bond length is extended beyond *ca.* 2.4 Å, spin contamination becomes significant and a multi-configuration method will probably be required to map out this region of the potential energy curve. However, this is beyond the scope of the present work. We can therefore only offer an estimate for this barrier, based on the last points without significant spin contamination, but it is more than 50 kJ mol^{-1} for the fluorine reaction. For the chlorine reaction, the CH_2ClO formation is already endothermic and the calculated barrier to the products, ClCHO and H, is a formidable 115.4 kJ mol^{-1}. We therefore conclude that the reaction X + HCHO → H + XHCO is unimportant for all halogen atoms at room temperature.

For the halogen atom reactions with acetaldehyde we limited the study to reaction path (VIIb),

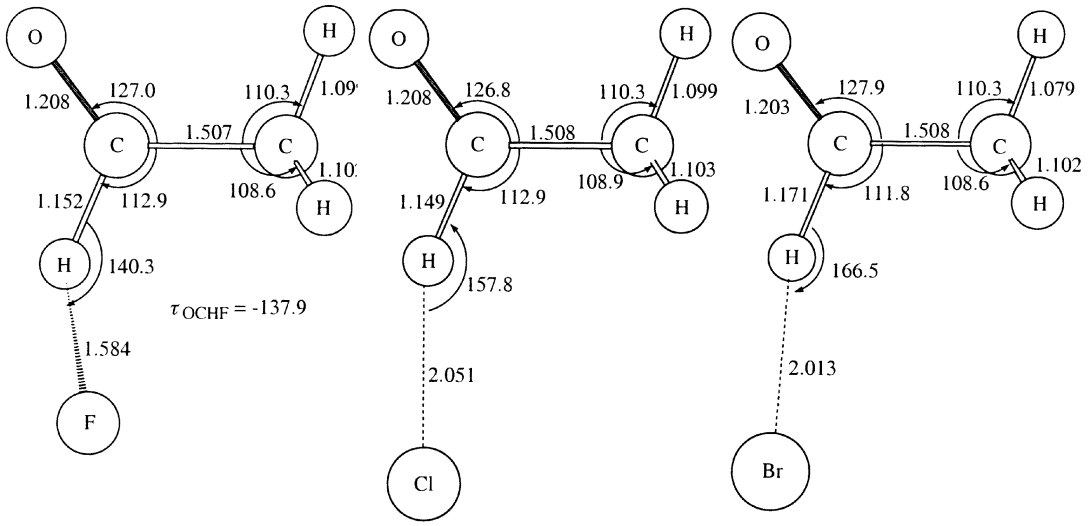

E_{MP2} = -252.898772
ΔE_{elec} = 8.7 kJ mol^{-1}
$i\varpi$ = −534 cm^{-1}

E_{MP2} = -612.965833
ΔE_{elec} = 3.6 kJ mol^{-1}
$i\varpi$ = −148 cm^{-1}

E_{MP2} = -2725.857193
ΔE_{elec} = 5.6 kJ mol^{-1}
$i\varpi$ = −145 cm^{-1}

Fig. 11 Structures and electronic energies (in E_h) of the transition states in the reactions; X + CH_3CHO → CH_3CO + HX; X = F, Cl, Br. The F–H–C=O arrangement is non-planar.

$X + CH_3CHO \rightarrow HX + CH_3CO$. The transition states are depicted in Fig. 12, which also includes the electronic energies and energy differences relative to the reactants. As in the case of the F···HCHO transition state, also the $CH_3C(O)H\cdots F$ transitions state has a non-planar F···H–C(O)–R arrangement with a small barrier of *ca.* 0.5 kJ mol^{-1} in the C_s configuration.

Calculation of reaction rate coefficients

The reaction rate coefficients were calculated from the generalised transition state theory:

$$k(T) = \sigma \frac{k_B T}{h} \frac{Q^{TS}(T)}{Q^{R}(T)} \times \exp\left(-\frac{(E^{TS}_{elec} + E^{TS}_0) - (E^{R}_{elec} + E^{R}_0)}{k_B T}\right) \quad (2)$$

where σ is a symmetry factor accounting for the possibility of more than one symmetry-related reaction path-σ is 2 for the formaldehyde and 1 for the acetaldehyde reactions. k_B is Boltzmann's constant, h is Planck's constant, E_{elec} is the electronic energy and E_0 the vibration zero-point energy. $Q^{TS}(T)$ and $Q^{R}(T)$ are, respectively, the internal partition function at the generalised transition state, and the reactants partition function per unit volume. These functions, in turn, are approximated as products of electronic, rotation, vibration and translation partition functions. The translation and rotation partition functions can be treated classically; the vibration partition functions were calculated in the harmonic oscillator approximation using the results from quantum mechanics. For the non-planar fluorine–formaldehyde transition state, the F–H–C=O torsional vibration was also treated as a free internal rotor. The methyl torsion in the acetaldehyde systems was treated as the other modes since the effects of hindered rotation will almost completely cancel in eqn. (2). For the sake of brevity we only give the imaginary wavenumber of the reaction co-ordinate as calculated from the Hessian matrix, and do not present all the calculated vibrational wavenumbers of the reactants and transition states, Fig. 9 and 11.

The calculated rate coefficients for the reactions of halogen atoms with formaldehyde and acetaldehyde are compared to literature data in the usual form of Arrhenius plots, log $k(T)$ *vs.* T^{-1}, in Fig. 12. The calculations are based on the results from the MP2/cc-pVDZ calculations, but for the fluorine and chlorine reactions with formaldehyde, we have included the

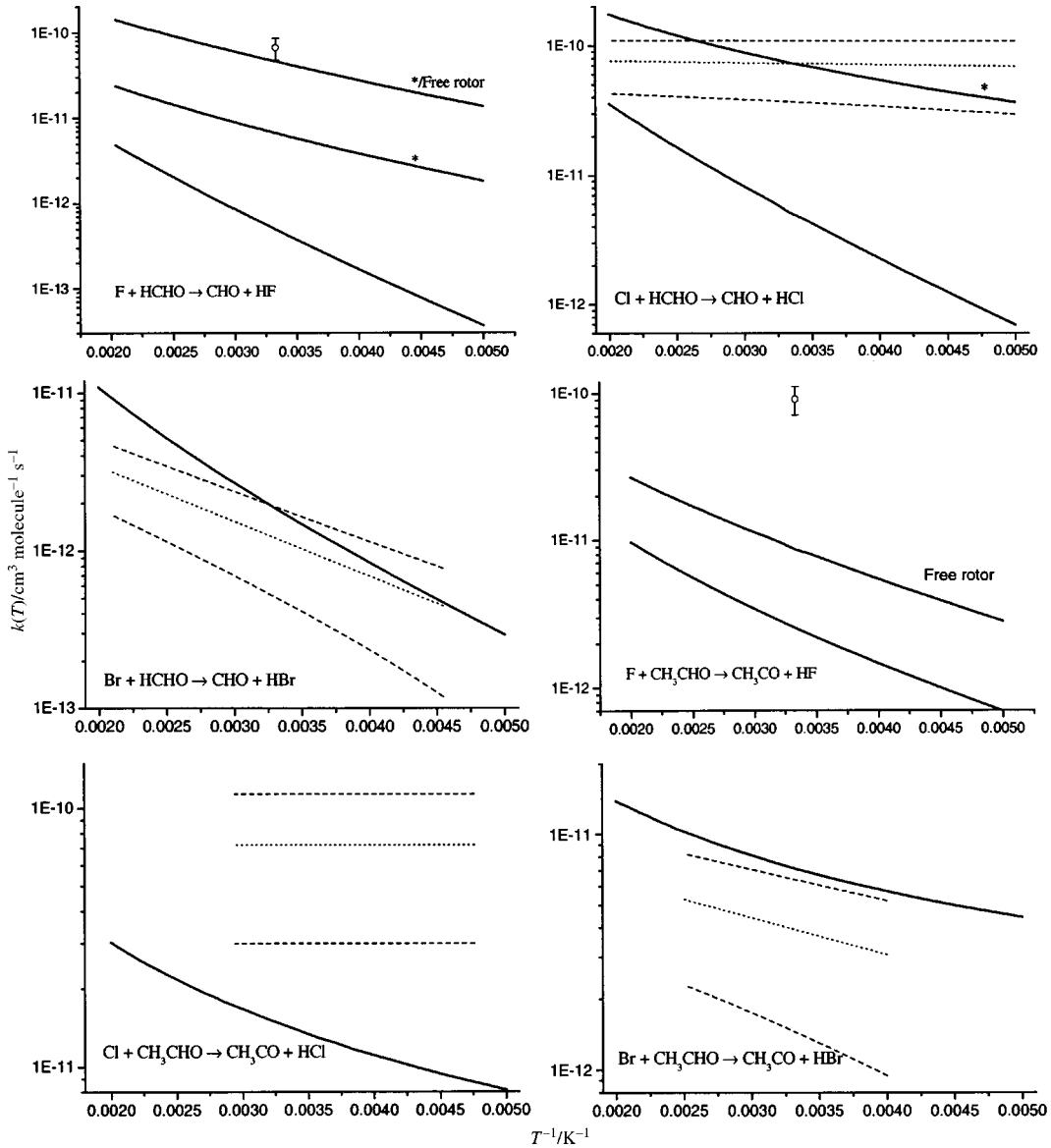

Fig. 12 Observed and calculated reaction rate coefficients for the reactions of F, Cl and Br with HCHO (top) and CH_3CHO (bottom). Observations are presented either as points with error bars or as dotted curves with error limits given by dashed curves. Calculations are given as full curves. Curves marked with asterisks are based on MP2(full)/aug-cc-pVDZ calculations. Curves marked by "Free Rotor" are based on calculations where the internal motion of the F–H–C=O entity around the H–C bond is treated as a free internal rotation.

results from the MP2(full)/aug-cc-pVDZ calculations as well (note the different scales in the plots of Fig. 12). For the fluorine reactions, Fig. 12 also includes the rate coefficient resulting from a model assuming free internal rotation around the H–C bond of the F–H–C=O entity. In general, there is a clear curvature on the calculated rate coefficient plots. In fact, the pre-exponential factors of the rate coefficients are in all cases reasonably well approximated by the expression $A \times T^n$ in the temperature region from 200 to 500 K.

The experimental data for the fluorine reactions are scarce; the kinetics of the reaction F + HCHO has only been the subject of one study, a room-temperature study by the discharge flow reactor–EPR method,[7] giving $k_{298} = 6.6 \times 10^{-11}$ cm^3 molecule^{-1} s^{-1}. The calculated rate coefficient, obtained from MP2/cc-pVDZ calculations, is two orders of magnitude smaller. By including diffuse functions in the basis sets, the predicted barrier to reaction is lowered, and the reaction rate coefficient increases correspondingly. As mentioned previously, the F···HCHO transition state has a non-planar structure with a low barrier to internal rotation. Replacing the harmonic contribution to the partition function from this mode by that of a free internal rotor increases the pre-exponential factor by an order of magnitude and results in a very good agreement with the single experiment, Fig. 12. Although this is a crude first approximation, the result does not differ significantly from that of a more rigorous treatment.[58] According to the theoretical results (MP2(full)/aug-cc-pVDZ and free internal rotation of the F–H–C=O entity around the H–C bond) the rate coefficient can be approximated by: $k_T = 6.0 \times T^{0.70} \times 10^{-12} \times \exp(-590/T)$ and $k_{298} = 4.5 \times 10^{-11}$ cm^3 molecule^{-1} s^{-1}.

The kinetics of the Cl + HCHO reaction was studied at room temperature by the relative rate technique using FTIR,[8] by infrared chemiluminescence following laser induced generation of Cl atoms,[9] by discharge flow–mass spectrometry,[10] by discharge flow–EPR[14] and by flash photolysis–resonance fluorescence.[11] Two temperature studies, both by flash photolysis–resonance fluorescence, have been reported.[12,13] The recommended reaction rate coefficient is: $k_T = 8.2 \times 10^{-11} \times \exp(-34/T)$ and $k_{298} = 7.3 \times 10^{-11}$ cm^3 molecule^{-1} s^{-1},[45] that is, virtually without temperature dependence. The theoretical results give a much larger temperature dependence, Fig. 12, although the general prediction based upon MP2(full)/aug-cc-pVDZ calculations show a better agreement. The calculated rate coefficient, obtained from MP2(full)/aug-cc-pVDZ calculations, can be approximated by: $k_T = 1.21 \times T^{1.22} \times 10^{-13} \times \exp(-135/T)$ and $k_{298} = 8.0 \times 10^{-11}$ cm^3 molecule^{-1} s^{-1}.

The Br + HCHO reaction was studied at room temperature using the discharge flow reactor–EPR method,[7] and later over a wide temperature range by flash photolysis–resonance fluorescence[15] and discharge flow–mass spectrometry.[10] The modelled rate coefficient, Fig. 12 is, perhaps fortuitously, close to the recommended value, $k_T = 1.7 \times 10^{-11} \times \exp(-800/T)$ and $k_{298} = 1.1 \times 10^{-12}$ cm^3 molecule^{-1} s^{-1}.[45] Even the temperature dependence is reproduced in a fair manner, $k_T = 8.42 \times T^{1.07} \times 10^{-14} \times \exp(-900/T)$ and $k_{298} = 1.8 \times 10^{-12}$ cm^3 molecule^{-1} s^{-1}. Nava *et al.*[15] estimated the temperature dependence of the reaction rate coefficient from transition state theory assuming a co-linear C–H–Br structure of the activated complex. Their calculation is somewhat difficult to reproduce, but they also predicted a curved Arrhenius plot.

The F + CH_3CHO kinetics were studied at room temperature by flow-tube discharge[18,19] and by pulse-radiolysis employing UV–VIS detection.[17] In the latter study two reaction channels, (VIIb) and (VIId), were inferred from the transient UV spectra, with $65 \pm 9\%$ passing through (VIIb) and giving $k_{298} = 9.1 \times 10^{-11}$ cm^3 molecule^{-1} s^{-1} for the F + $CH_3CHO \rightarrow$ HF + CH_3CO reaction. Fig. 12 shows two curves obtained for the reaction rate coefficient. The curve based on the assumption of all internal motions being harmonic deviates by more than an order of magnitude from experiment. Improved agreement is obtained by including free internal rotation of the F–H–C=O entity around the H–C bond: $k_T = 3.8 \times T^{0.84} \times 10^{-13} \times \exp(-501/T)$ cm^3 molecule^{-1} s^{-1}. It is obvious that a mere reduction in the potential energy barrier to reaction, similar to that obtained for the formaldehyde system by including diffuse functions in the *ab initio* calculations, will bring the theoretical reaction rate coefficient close to the experiment.

The Cl + CH_3CHO and Br + CH_3CHO reactions were studied by several methods: Cl,[12,20–24] and Br.[25–31] The observed rate coefficients for these reactions show an even more pronounced lack of temperature dependence than the corresponding formaldehyde coefficients; the recommended value for chlorine reaction is constant over the temperature range studied, $k = 7.2 \times 10^{-11}$ and $k_T = 1.3 \times 10^{-15} \times \exp(-360/T)$ cm^3 molecule^{-1} s^{-1} for the bromine reaction.[45] The calculated rate coefficients show clear temperature variations and can be approximated by $k_T = 1.07 \times T^{1.29} \times 10^{-14} \times \exp(-51/T)$ and $k_T = 7.90 \times T^{1.21} \times 10^{-15} \times \exp(-24/T)$ cm^3 molecule^{-1} s^{-1} for chlorine and bromine, respectively. As noted above, adding diffuse functions in the *ab initio* calculations is expected to result in a reduction in the calculated barrier to reaction for chlorine and consequently to bring the derived reaction rate coefficients closer to observations.

Kinetic isotope effects

Following the conventional transition state model, the kinetic isotope effect, $KIE_{\alpha,\beta}$, defined as the ratio between the reaction rate coefficients of isotopomers α and β with the same reactant, has two origins. First, there is a contribution from the changes in the partition functions caused by the isotopic substitution. Second, there is a contribution from the exponential factor caused by changes in the vibrational zero-point energies upon isotope substitution.

$$KIE_{\alpha,\beta}(T) = \frac{Q_\alpha^{TS}(T) Q_\beta^{R}(T)}{Q_\alpha^{TS}(T) Q_\beta^{TS}(T)} \times \exp\left(- \frac{(E_{0,\alpha}^{TS} - E_{0,\alpha}^{R}) - (E_{0,\beta}^{TS} - E_{0,\beta}^{R})}{k_B T} \right) \quad (3)$$

The $KIE_{\alpha,\beta}$ can thus be written as a product of three terms—translational, rotational and vibrational, the first two being independent of temperature. The translational term depends only upon the reduced masses of the isotopomer reactants and will be close to unity, the rotational term depends only upon the rotational constants of reactants and transition states, and the vibrational term is essentially dominated by the low-lying vibrational modes. For the formaldehyde–halogen atom systems, the contributions to $KIE_{HH,DD}$ from the partition functions are 1.35, 1.09 and 1.16, for F, Cl and Br, respectively, while the major contributions to $KIE_{HH,DD}$ are from the changes in zero-point energies: 2.12, 2.30 and 4.92 at 298 K. The rather dramatic change in description of internal motion on going from a harmonic torsional mode in the F···HCHO system to a free internal rotation, makes little difference in the calculated $KIE_{HH,DD}$. The calculated kinetic isotope effects are compared to the observations in Table 4. As can be seen, the agreement is not particularly impressive although one may claim that the trends are correct.

Adducts

The computational results indicate that there exist weak but stable adducts between halogen atoms and formaldehyde, in which the halogen atom is bonded to the oxygen atom of the carbonyl group. Although not calculated yet, the halogen atoms are also expected to form similar type adducts with acetaldehyde and higher aldehydes. Calculations show that

there are a substantial number of bound vibrational states of the halogen atom adducts. In the harmonic oscillator model of the fluorine–formaldehyde system, there are fewer bound vibrational states than in the analogous chlorine and bromine systems, and the effect of adduct formation may be less effective in promoting reaction.

Conclusion

The experimental product studies indicate that Cl and Br only react with formaldehyde through hydrogen abstraction, $X + HCHO \rightarrow HX + HCO$. The theoretical studies indicate that barriers in the substitution reaction, $X + HCHO \rightarrow H + XHCO$, are too high for both F and Cl to occur at room temperature. For acetaldehyde, the dominating reaction with Cl is the aldehydic hydrogen abstraction, $X + CH_3CHO \rightarrow HX + CH_3CO$.

The computational results indicate that the halogen atom reactions with formaldehyde and acetaldehyde (and likely with higher aldehydes as well) all proceed in the same fashion *via* similar transition states and all with reaction rate coefficients having a comparable temperature dependence. It is therefore at first sight surprising that the chlorine reactions show virtually no temperature dependence and that the bromine reactions only have a small, but clear temperature dependence. The existence of adducts between the aldehydes and the halogen atoms, with corresponding attractive potentials, will increase the calculated reaction coefficients, the fluorine system should be the least effected. The importance of this attraction will decrease as the kinetic energy increases, that is, with increasing temperature. The apparent temperature dependence of the reaction will therefore be less than calculated by transition state theory, in agreement with the observations for both the chlorine and bromine reactions. As the fluorine reactions should be the least affected and because the transition states of the fluorine–aldehyde reactions differ from the analogous chlorine and bromine reactions by having non-planer F–H–C=O arrangements, it will be of interest to have temperature studies of these reaction rate coefficients.

Conventional transition state theory can only explain the observed kinetic isotope effects in part. In fact, the agreement with the experimental results is somewhat unsatisfactory. The predicted kinetic isotope effects of the fluorine–aldehyde reactions are quite large and, for the same reasons as stated above, it will be of interest to have these experimental reference data available for further theoretical development. It is likely that variational transition state theory and the inclusion of quantum mechanical tunnelling effects to some extent will reduce the gap between theory and experiment, and work along these lines are in progress.

Acknowledgement

This work is part of the project "Carbonyls in Tropospheric Oxidation Mechanisms" (CATOME) and has received support from The Research Council of Norway (Programme for Supercomputing) through a grant of computing time, and from the CEC Environment and Climate program through contract ENV4-CT97-0416. BDA acknowledges financial support from The Research Council of Norway through grant no. 123289/410.

References

1 D. Kotzias, C. Konidara and C. Spartà, in *Biogenic Volatile Organic Compounds in the Atmosphere—Summary of Present Knowledge*, ed. G. Helas, S. Slanina and R. Steinbrecher, SPB Academic Publishers, Amsterdam, 1997, p. 67.
2 B. P. Shepson, A.-P. Sirju, J. F. Hopper, L. A. Barrie, V. Young, H. Niki and H. Dryfhout, *J. Geophys. Res.*, 1996, **101**, 21081.
3 L. A. Barrie, J. W. Bottenheim, C. Schnell, P. J. Crutzen and R. A. Rasmussen, *Nature*, 1998, **334**, 138.
4 Y. L. Yung, J. P. Pinto, R. T. Watson and S. P. Sander, *J. Atmos. Sci.*, 1980, **37**, 339.
5 B. D'Anna and C. J. Nielsen, *J. Chem. Soc., Faraday Trans.*, 1997, **93**, 3479.
6 B. D'Anna, J. A. Beukes, M. Giannouli and C. J. Nielsen, *FZK Proc*, **98(01)**, 1998.
7 G. Le Bras, R. Foon and J. Combourieu, *Chem. Phys. Lett.*, 1980, **73**, 357.
8 H. Niki, P. D. Maker, L. P. Breitenbach and C. M. Savage, *Chem. Phys. Lett.*, 1978, **57**, 596.
9 D. M. Fasano and N. S. Nogar, *Int. J. Chem. Kinet.*, 1981, **13**, 325.
10 G. Poulet, G. Laverdet and G. Le Bras, *J. Phys. Chem.*, 1981, **85**, 1892.
11 J. J. Stief, J. V. Michael, W. A. Payne, D. F. Nava, D. M. Butler and R. S. Stolarski, *Geophys. Res. Lett.*, 1978, **5**, 829.
12 J. V. Michael, D. F. Nava, W. A. Payne and L. J. Stief, *J. Chem. Phys.*, 1979, **70**, 1147.
13 P. C. Anderson and M. J. Kurylo, *J. Phys. Chem.*, 1979, **83**, 2055.
14 R. Foon, G. Le Bras and J. Combourieu, *C. R. Acad. Sci. Paris*, 1979, **288**, 241.
15 D. F. Nava, J. V. Michael and L. J. Stief, *J. Phys. Chem.*, 1981, **85**, 1896.
16 J. A. Beukes, B. D'Anna and C. J. Nielsen, *Asian Chem. Lett.*, 2000, **4**, 145.
17 J. Sehested, L. K. Christensen, O. J. Nielsen and T. Wallington, *Int. J. Chem. Kinet.*, 1998, **30**, 913.
18 D. J. Smith, D. W. Setzer, J. C. Kim and D. J. Bogan, *J. Phys. Chem.*, 1977, **81**, 898.
19 M. Bartels and K. Hoyermann, *An. Asoc. Quim. Argent.*, 1985, **73**, 253.
20 D. J. Scollard, J. J. Treacy, H. W. Sidebottom, C. Balestra-Garcia, G. Laverdet, G. Le Bras, H. Mac Leod and S. Téton, *J. Phys. Chem.*, 1993, **97**, 4683.
21 W. A. Payne, D. F. Nava, F. L. Nesbitt and L. J. Stief, *J. Phys. Chem.*, 1990, **94**, 7190.
22 H. Niki, P. D. Maker, C. M. Savage and L. P. Breitenbach, *J. Phys. Chem.*, 1985, **89**, 588.
23 T. J. Wallington, L. M. Skewes, W. O. Siegel, C.-H. Wu and S. M. Japar, *Int. J. Chem. Kinet.*, 1988, **20**, 867.
24 M. Bartels, K. Hoyermann and U. Lange, *Ber. Bunsen-Ges Phys. Chem.*, 1989, **93**, 423.
25 J. M. Nicovich, C. J. Shackelford and P. H. Wine, *J. Photochem. Photobiol., A: Chemistry*, 1990, **51**, 141.
26 T. S. A. Islam, R. M. Marshall and S. W. Benson, *Int. J. Chem. Kinet.*, 1984, **16**, 1161.
27 H. Niki, P. D. Maker, C. M. Savage and L. P. Breitenbach, *Int. J. Chem. Kinet.*, 1985, **17**, 525.
28 I. Barnes, V. Bastian, K. H. Becker, R. Overath and Z. Tong, *Int. J. Chem. Kinet.*, 1989, **21**, 499.
29 T. J. Wallington, L. M. Skewes, W. O. Siegl and S. M. Japar, *Int. J. Chem. Kinet.*, 1989, **21**, 1069.
30 I. Szilágyi, K. Imrik, S. Dóbé and T. Bérces, *Ber. Bunsen-Ges Phys. Chem.*, 1998, **102**, 79.
31 B. Ramacher, J. J. Orlando and G. S. Tyndall, *Int. J. Chem. Kinet.*, 2000, **32**, 460.
32 M. J. Frisch, G. W. Trucks, H. B. Schlegel, G. E. Scuseria, M. A. Robb, J. R. Cheeseman, V. G. Zakrzewski, J. A. Montgomery, Jr., R. E. Stratmann, J. C. Burant, S. Dapprich, J. M. Millam, A. D. Daniels, K. N. Kudin, M. C. Strain, O. Farkas, J. Tomasi, V. Barone, M. Cossi, R. Cammi, B. Mennucci, C. Pomelli, C. Adamo, S. Clifford, J. Ochterski, G. A. Petersson, P. Y. Ayala, Q. Cui, K. Morokuma, D. K. Malick, A. D. Rabuck, K. Raghavachari, J. B. Foresman, J. Cioslowski, J. V. Ortiz, A. G. Baboul, B. B. Stefanov, G. Liu, A. Liashenko, P. Piskorz, I. Komaromi, R. Gomperts, R. L. Martin, D. J. Fox, T. Keith, M. A. Al-Laham, C. Y. Peng, A. Nanayakkara, C. Gonzalez, M. Challacombe, P. M. W. Gill, B. Johnson, W. Chen, M. W. Wong, J. L. Andres, C. Gonzalez, M. Head-Gordon, E. S. Replogle and J. A. Pople, Gaussian, Inc., Pittsburgh, PA, 1998.
33 C. Møller and M. S. Plesset, *Phys. Rev.*, 1934, **46**, 618.
34 M. Head-Gordon, J. A. Pople and M. J. Frisch, *Chem. Phys. Lett.*, 1988, **153**, 503.
35 M. J. Frisch, M. Head-Gordon and J. A. Pople, *Chem. Phys. Lett.*, 1990, **166**, 275.
36 M. J. Frisch, M. Head-Gordon and J. A. Pople, *Chem. Phys. Lett.*, 1990, **166**, 281.
37 M. Head-Gordon and T. Head-Gordon, *Chem. Phys. Lett.*, 1994, **220**, 122.
38 G. W. Trucks, M. J. Frisch, J. L. Andres and H. B. Schlegel, in preparation.

39 S. Saebo and J. Almlof, *Chem. Phys. Lett*., 1989, **154**, 83.
40 D. E. Woon and T. H. Dunning, Jr., *J. Chem. Phys*., 1993, **98**, 1358.
41 R. A. Kendall, T. H. Dunning, Jr. and R. J. Harrison, *J. Chem. Phys*., 1992, **96**, 6796.
42 T. H. Dunning, Jr., *J. Chem. Phys*., 1989, **90**, 1007.
43 K. A. Peterson, D. E. Woon and T. H. Dunning, Jr., *J. Chem. Phys*., 1994, **100**, 7410.
44 A. Wilson, T. van Mourik and T. H. Dunning, Jr., *J. Mol. Struct*. (*Theochem*), 1997, **388**, 339.
45 R. Atkinson, D. L. Baulch, R. A. Cox, R. F. Hampson, Jr., J. A. Kerr, M. J. Rossi and J. Troe, *J. Phys. Chem. Ref. Data*, 1997, **26**, 521.
46 F. Su, J. G. Calvert and J. H. Shaw, *J. Phys. Chem*., 1979, **83**, 3185.
47 J. P. Burrows, G. K. Moortgat, G. S. Tyndall, R. A. Cox, M. E. Jenkin, G. D. Hayman and B. Veyret, *J. Phys. Chem*., 1989, **93**, 2375.
48 B. Veyret, R. Lesclaux, M.-T. Rayez, J.-C. Rayez, R. A. Cox and G. K. Moortgat, *J. Phys. Chem*., 1989, **93**, 2368.
49 F. Zabel, K. A. Sahetchian and C. Chachaty, *Chem. Phys. Lett*., 1987, **134**, 433.
50 I. Barnes, K. H. Becker, E. H. Fink, F. Zabel and H. Niki, *Chem. Phys. Lett*., 1985, **115**, 1.
51 F. Su, J. G. Calvert, J. H. Shaw, H. Niki, P. D. Maker, C. M. Savage and L. D. Breitenbach, *Chem. Phys. Lett*., 1979, **65**, 221.
52 B. Veyret, J.-C. Rayez and R. Lesclaux, *J. Phys. Chem*., 1982, **86**, 3424.
53 D. York, *Can. J. Phys*., 1966, **44**, 1079.
54 FACSIMILE release 3.610000, Date 14/07/98, 1998, AEA Technology plc.
55 W. G. Mallard, F. Westley, J. T. Herron and R. F. Hampson, NIST Chemical Kinetics Database-Ver. 6.0, NIST Standard Reference Data, Gaithersburg, MD, 1994.
56 W. B. DeMore, S. P. Sander, D. M. Golden, R. F. Hampson, M. J. Kurylo, C. J. Howard, A. R. Ravishankara, C. E. Kolb and M. J. Molina, *Jet Propul. Lab. Publ. 97-4*, 1997.
57 B. D'Anna, V. Bakken, J. A. Beukes and C. J. Nielsen, to be published.
58 D. G. Truhlar, *J. Comput. Chem*., 1991, **12**, 266.